A Benchmarking Tool for MAV Visual Pose Estimation

Gim Hee Lee*, Markus Achtelik†, Friedrich Fraundorfer*, Marc Pollefeys*, and Roland Siegwart†
*Computer Vision and Geometry Laboratory, Department of Computer Science, ETH Zürich
†Autonomous Systems Laboratory, Department of Mechanical Engineering, ETH Zürich
glee@student.ethz.ch, markus.achtelik@mavt.ethz.ch, fraundorfer@inf.ethz.ch, marc.pollefeys@inf.ethz.ch, rsiegwart@ethz.ch

***Abstract*—The large collections of datasets for researchers working on the Simultaneous Localization and Mapping problem are mostly collected from sensors such as wheel encoders and laser range finders mounted on ground robots. The recent growing interest in doing visual pose estimation with cameras mounted on micro-aerial vehicles however has made these datasets less useful. In this paper, we describe our work in creating new datasets collected from a sensor suite mounted on a quadrotor platform. Our sensor suite includes a forward looking camera, a downward looking camera, an inertial measurement unit and a Vicon system for groundtruth. We propose the use our datasets as benchmarking tools for future works on visual pose estimation for micro-aerial vehicles. We also show examples of how the datasets could be used for benchmarking visual pose estimation algorithms.**

***Index Terms*—Micro-Aerial Vehicles, Quadrotor, Visual SLAM, Benchmarking Tool.**

I. INTRODUCTION

Over the past two decades, the problem of Simultaneous Localization and Mapping (SLAM) for ground robots has been actively researched on by a large number of researchers [5]–[7]. In many cases, the most convenient way to assess a SLAM algorithm would be to test it on offline datasets collected from a sensor suite mounted on the robot which was driven through the environment. This approach has made it easier for researchers to focus on algorithm developments while eliminating hardware and data synchronization issues. Robot trajectories and maps produced from the SLAM algorithms are usually benchmarked against architectural blueprints for indoor environments or global positioning system (GPS) for outdoor environments. Consequently, a large number of repositories hosting these offline datasets could be found [1]–[3]. The most common sensor suite consists of the inertial measurement units (IMUs), wheel encoders, laser range finders, ultra-sonic sensors, and GPS for outdoor environments.

In the recent years, the research focus of SLAM is gradually moving towards using cameras as the main sensor [9], [10]. This is largely due to the fact that the 2D laser range finder, which has been the most popular choice for doing SLAM on ground robots, could only provide very limited information from its planar point cloud readings. In contrast, images obtained from cameras could be used to extract 3D information of the environment, and more importantly, rich information given by the color and pixel intensity could also be used for scene recognition which has been proven to be more superior for the detection of loop closure opportunities [8]. In even more recent years, there is a strong growing interest among various research groups on using Micro-Aerial Vehicles (MAVs) for autonomous navigation in challenging environments due to its locomotive advantages over ground robots. Higher maneuverability and limited payload of flying robots imply that cameras would be a nature choice for its main sensor.

However, the paradigm shift in the robotics platforms and sensors means that the large collections of offline datasets, which are available in many repositories, for SLAM would no longer be useful. Hence, in this paper we describe our work on creating datasets collected from a sensor suite mounted on a MAV as a benchmarking tool for MAV visual pose estimation. Our sensor suite includes a forward looking and a downward looking camera, an IMU unit with 3 axis gyroscopes, 3 axis accelerometers and a magnetometer, and a Vicon system. Pose measurements from the Vicon system are used as the groundtruth which is very useful for benchmarking visual pose estimation of a MAV flying in indoor environments where it would be impossible to justify using 2D architectural blueprints. In addition, ARToolKitPlus markers [14], which can be used to estimate the camera poses, are placed on known positions on the ground and the flightpaths are choreographed to ensure that the markers are always within the line-of-sight of the downward looking camera.

The paper is structured as follows. In Section II, we describe our MAV platform and the sensor suite used for data collection as well as the environment setup. In Section III, we describe the procedures for synchronizing the readings collected from different sensors. We will also discuss about the camera calibration procedures. In Section IV, we describe the content of the benchmarking datasets and provide information on how to obtain a copy of it. Finally, in Section V, we show examples of the usage of our dataset to quantify existing visual pose estimation algorithms such as the 5-point algorithm [15], 4-point algorithm [18] and ARToolKitPlus [14] compared to the groundtruth from the Vicon system.

II. MAV Platform and Environment Setup

Figure 1(a) shows a “Pelican” quadrotor from Ascending Technologies [1] which we used for data collection. The quadrotor has an inbuilt MEMS IMU equipped with 3 axis gyroscopes, 3 axis accelerometers and a magnetometer which respectively gives the measurements of the attitude rates, accelerations and absolute heading. A filter within the IMU

[1] http://www.asctec.de/

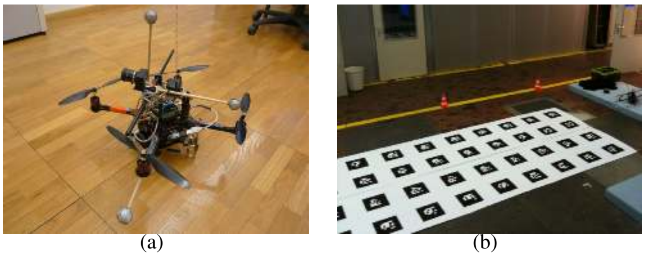

(a) (b)

Fig. 1. (a) The "Pelican" quadrotor equipped with a forward looking camera, a downward looking camera, an IMU, and three reflective markers for the Vicon system. (b) Group of ARToolKitPLus markers placed in known location.

fuses the attitude rates, accelerations and heading at a rate of 1KHz to give absolute attitude measurements.

For our objective of visual pose estimation, we added a forward looking and a downward looking camera. Both cameras are PointGrey USB-Firefly [2] cameras which run at a maximum framerate of 30 frames per second. The forward looking camera is equipped with a 6mm CS-mount lens with 80° field of view and the downward looking camera has a fisheye lens with 150° field of view to increase the coverage.

The IMU and the cameras are connected to an onboard computer providing UART and USB interfaces. This computer is equipped with a 1.6GHz Intel Atom processor and 1GB RAM and thus is able to run standard x86 operating systems such as Ubuntu 9.10 in our case.

For data-capturing, we make use of the ROS [4] framework. We wrote nodes to receive IMU data over a serial interface at 200Hz as well as for capturing images from the cameras. These nodes publish IMU- and image-messages that are logged into binary "bag"-files onto a USB stick using the ROS-tool "rosbag" and are later exported via scripts to matlab-files. Furthermore, to have a preview, images are streamed at lower quality via a wireless 802.11n connection to a laptop serving as ground station.

The quadrotor was flown in a 10m×10m×10m indoor environment equipped with eight Vicon cameras mounted on the four sides of the ceiling walls. Three reflective markers are mounted asymmetrically and rigidly onto the quadrotor for the motion capture. Pose estimation from the Vicon system is performed at a separate computer system at a precise frequency of 200Hz. Furthermore, a group of ARToolkit markers is placed on the floor at known locations with respect to the Vicon coordinate origin. Figure 1(b) shows the group of ARToolKitPLus markers used in our setup. The ARToolKitPLus was originally created for tracking camera poses in the augmented reality applications, but is used in our experimental setup for enhancing features on the floor for the images.

III. Data Synchronization and Camera Calibration

A. Data Synchronization

The camera images, Vicon and IMU data are not useful for benchmarking visual pose estimation algorithms on MAVs unless they are perfectly synchronized. There are no synchronization issues between the camera and IMU since these data were captured on the same computer evaluating embedded timestamps from the respective hardware. Synchronization between the Vicon system and IMU/camera poses a problem since these data were collected on different computers. The IMU and Vicon data however could not be synchronized by direct comparison because the IMU measures the attitude rates in the body frame but the Vicon system measures the Euler angles with respect to its frame of reference. We therefore took the advantage of the precise sampling rate of the Vicon system to overcome this problem. We would differentiate the Euler angles and transform them into the body frame. Equation 1 shows the relationship between the attitude rates (p, q, r) in the body frame and the Euler angles (ϕ, θ, ψ). f_v is the frequency of the Vicon system.

$$\begin{pmatrix} p \\ q \\ r \end{pmatrix} = f_v \begin{pmatrix} 1 & 0 & -sin(\theta) \\ 0 & cos(\phi) & cos(\theta)sin(\phi) \\ 0 & -sin(\phi) & cos(\theta)cos(\phi) \end{pmatrix} \begin{pmatrix} \Delta\phi \\ \Delta\theta \\ \Delta\psi \end{pmatrix} \tag{1}$$

Figure 2 shows the IMU and Vicon roll and pitch angular rates in the body frame. Both data are clearly out of phase from each other. To synchronize the IMU and Vicon data, we create distinctive attitude rate profiles before and after flying the quadrotor by manually rotating the quadrotor around the roll and pitch directions respectively. We would then do a cross-correlation between the two data to find the time-shift between them. Figure 3 shows the correlation coefficients plot for both roll and pitch angular rates.

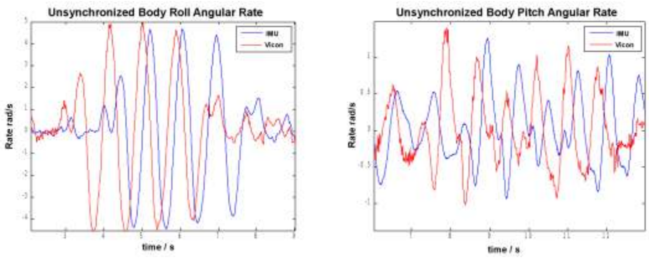

Fig. 2. Unsynchronized Vicon and IMU roll and pitch angular rates in the body frame.

Finally, we generate the synchronized data by compensating for the time-shift. An important factor to note is that cross-correlation in the discrete domain requires the signals to have the same sampling interval. We ensure that both the Vicon and IMU data have the same sampling intervals by cubic spline interpolation. Figure 4 shows the IMU and Vicon roll and pitch angular rates after synchronization. It is interesting to note that the cross-correlation done for both roll and pitch angular rates also results with a synchronization of the yaw angular rates as shown in Figure 5. This shows the accuracy of our synchronization method.

B. Camera Calibration

The first step to many visual algorithms is to find the camera intrinsic value and distortion coefficients. We have to

[2] http://www.ptgrey.com/products/fireflymv/index.asp

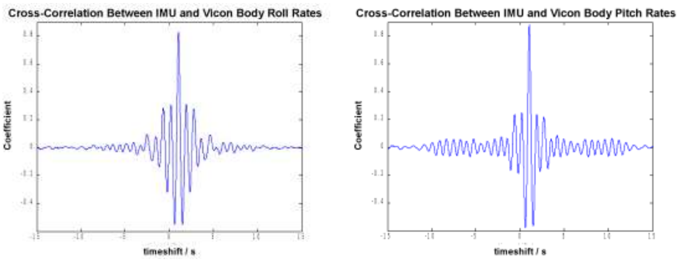

Fig. 3. Cross-correlation factors for unsynchronized roll and pitch body rates. The time-shift between two signals corresponds to the highest positive correlation.

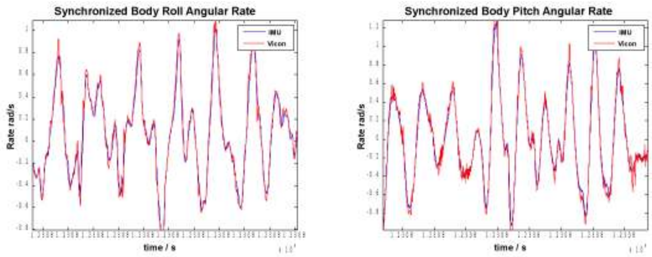

Fig. 4. IMU and Vicon roll and pitch angular rates after time synchronization.

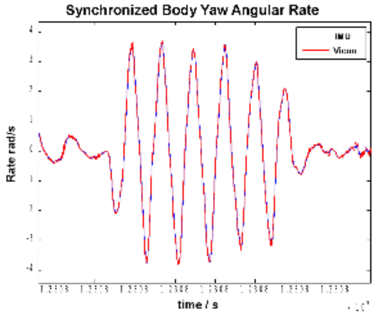

Fig. 5. IMU and Vicon yaw angular rates after time synchronization.

use two different camera calibration methods for the 6mm CS-mount lens and the fisheye lens due to the difference in the camera models. The “Bouguet Camera Calibration Toolbox” [11] and “Scaramuzza Omni-directional Camera Calibration Toolbox” [12], [13] were used to calibrate the 6mm CS-mount lens and the fisheye lens respectively. Both toolboxes provide functions to undistort the images after calibration. Figures 6 and 7 show examples of the calibration images before and after undistortion. It should be noted that the camera intrinsic values are not explicit results from the “Scaramuzza Omni-directional Camera Calibration Toolbox” for the fisheye lens. It must be computed from Equation 2 after the calibration and undistortion processes. sf is the zoom factor specified by the user during the undistortion process. The borders of an undistorted image usually contains artifacts, and sf determines the size of these borders to be removed after the undistortion process. i_w is the image width, and i_{wc} and i_{hc} are the image center coordinates.

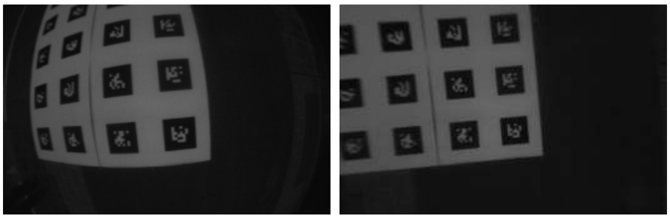

Fig. 6. Images from downward looking camera before and after undistortion.

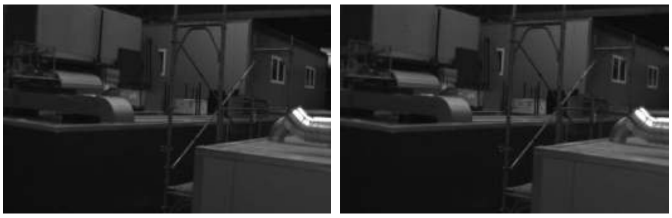

Fig. 7. Images from forward looking camera before and after undistortion.

$$K = \begin{pmatrix} \frac{i_w}{sf} & 0 & i_{wc} \\ 0 & \frac{i_w}{sf} & i_{hc} \\ 0 & 0 & 1 \end{pmatrix} \tag{2}$$

The transformation matrix ${}^{quad}T_{cam}$ that relates the camera frame to the quadrotor body frame in the Vicon system must be known for accurate comparison of any visual pose estimation with the Vicon system groundtruth. We made use of the Vicon system to find out ${}^{quad}T_{cam}$ since physical measurements will not give satisfactory results. Three Vicon reflective markers were fixed onto the image calibration board during the calibration process and this gives us the transformation ${}^{Vicon}T_{calib}$ that relates the calibration board frame to the Vicon frame. The reflective markers on the quadrotor body gives us the transformation ${}^{Vicon}T_{quad}$ that relates the quadrotor body frame to the Vicon frame. The transformation matrix ${}^{calib}T_{cam}$ can be obtained from the camera extrinsic values after the camera calibration and hence we are able to compute ${}^{quad}T_{cam}$ from Equation 3.

$${}^{quad}T_{cam} = inv({}^{Vicon}T_{quad}){}^{Vicon}T_{calib}{}^{calib}T_{cam} \tag{3}$$

IV. Benchmarking Dataset Package

Five synchronized datasets - 1LoopDown, 2LoopsDown, 3LoopsDown, hoveringDown and randomFront are created from this work. These datasets are collected from the quadrotor flying 1, 2 and 3 loop sequences, hovering within a space of approximately 1m×1m×1m, and flying randomly within the sight of the Vicon system. These datasets consist of images from the camera, accelerations, attitude rates, absolute angles and absolute headings from the IMU, and groundtruth from the Vicon system with their respective timestamps. Images from the first 4 datasets are from the downward looking camera and images from the last dataset are from the forward looking camera. Synchronized datasets for the calibrations of the forward and downward cameras are also provided.

We propose to measure the quality of any pose estimation algorithm with cosine similarity. The quality of each axis is measured separately, and the measurements for each of these axes could be obtained from the pose estimation algorithm and groundtruth as n-dimensional vectors denoted by E and G. The cosine similarity α is given by Equation 4 and has a range of $[-1\ 1]$ when the estimates exactly disagree or match the groundtruth. The matlab script that computes the cosine similarity is provided. Our datasets are available for download on http://projects.asl.ethz.ch/sfly/doku.php?id=mav_datasets.

$$\alpha = \frac{E.G}{\|E\|\,\|G\|} \tag{4}$$

V. Pose Estimation With Dataset

A. *Visual Odometry from the 5-point Algorithm*

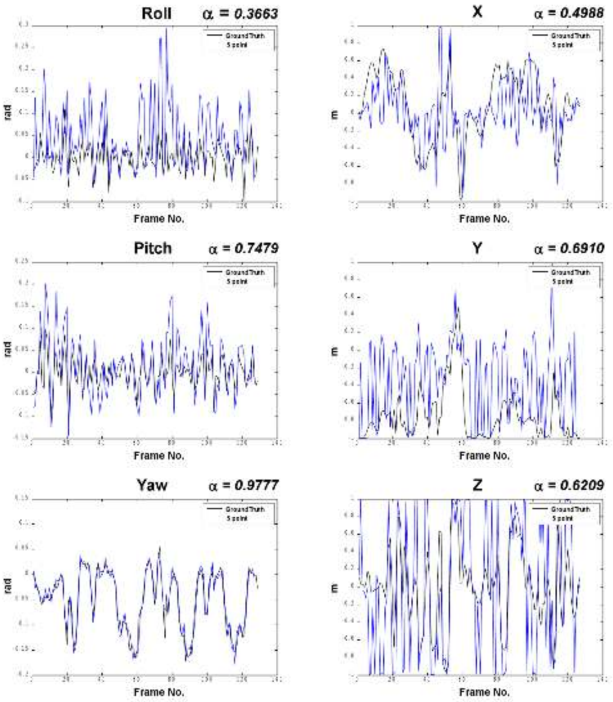

Fig. 8. Comparison of 5-point algorithm measurements to ground truth. The plots show roll, pitch, yaw, x, y, z values for 120 keyframes extracted from the 1LoopDown dataset. The high α value for yaw measurements shows that it is very accurate.

In this example, we computed the visual odometry using the 5-point algorithm for 120 keyframes extracted from the 1LoopDown dataset and compared it to the ground truth. First, we extracted the SIFT features [17] in all the keyframes and performed feature matching for each consecutive keyframe pair. Next, we computed the essential matrix using the 5-point algorithm [15] for each keyframe pair. Finally, the rotation matrix R and translation vector t that relates each image pair are extracted from the essential matrix. The RANSAC [16] algorithm is used for a more robust estimation of the essential matrix.

Figure 8 shows the comparison of the rotation and translation values. Each subplot shows the 5-point algorithm measurement (blue graphs) against the groundtruth measurement (black graphs). The translation vector t from both the 5-point algorithm and the groundtruth are normalized to unit length for better comparison. The α value for each axis is also computed. It is immediately visible from the plot and α value that the yaw measurements are most accurate. The accuracy of the yaw angle estimated by the 5-point algorithm can be explained by the downward looking camera where the yaw rotation is an in-plane rotation. The roll measurements has the lowest α value and therefore least accurate. The other measurements show a similar trend with the ground truth but are not exact.

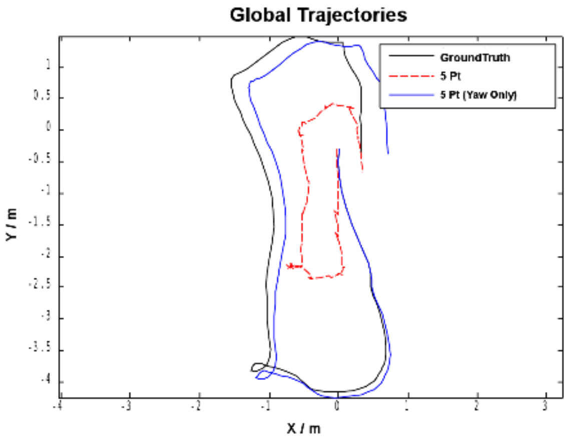

Fig. 9. Global trajectories from the 5-point algorithm (red dotted graph) and groundtruth (black graph) in the top view. The blue graph is the global trajectory computed with yaw values from the 5-point algorithm and remaining values from groundtruth.

Figure 9 shows the global trajectories from the 5-point algorithm (red dotted graph) and the groundtruth (black graph) in top view. The pair-wise transformations from the 5-point algorithm are concatenated to get the global trajectory. We scaled the translation vectors t with the groundtruth scale since we are only able to recover the relative scale from the 5-point algorithm. It can be seen that the global trajectory from the 5-point algorithm has a similar shape as the ground truth, but the length in the x and y directions are much shorter due to inaccuracy in the pose estimation. The blue graph shows the global trajectory computed with yaw values from the 5-point algorithm and remaining values from the groundtruth. This trajectory is very similar to the groundtruth because the yaw values from the 5-point algorithm are very accurate.

B. *Visual Odometry from the 4-point Algorithm*

Similar to the 5-point algorithm example, in this example we extracted 120 keyframes from the 1LoopDown dataset, and extracted SIFT matches [17] for each consecutive pair of keyframes. Next, we computed the homography for each consecutive pair of keyframes. For robust estimation, we used the 4-point RANSAC algorithm [16] to eliminate outliers followed by the Direct Linear Transformation algorithm [19] to estimate the homography with all the inliers. The relative pose (R and t) between each consecutive pair of keyframes is obtained by decomposing the homography [18]. This however gives 4 solutions where 2 are physically impossible and could

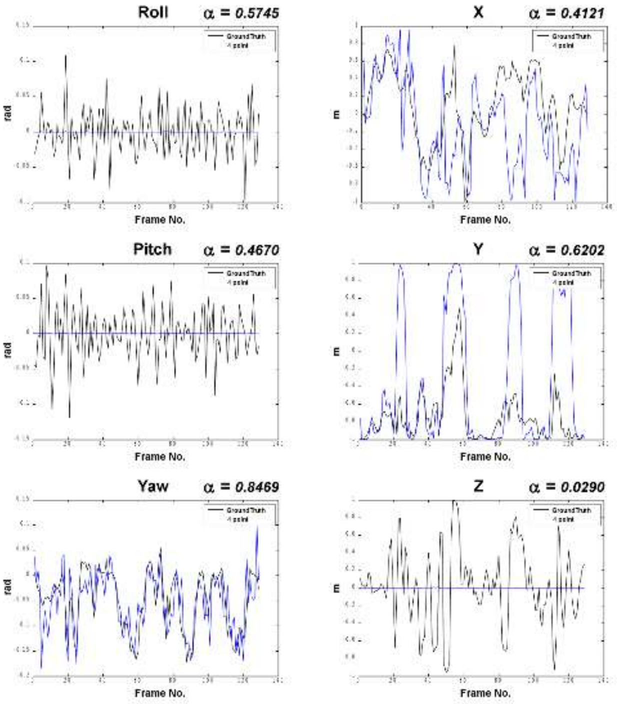

Fig. 10. Comparison of 4-point algorithm measurements to Vicon ground truth. The plots show roll, pitch, yaw, x, y, z values for 120 keyframes extracted from the 1LoopDown dataset. Similar to the 5-point algorithm, the yaw measurements is very accurate with a high α value.

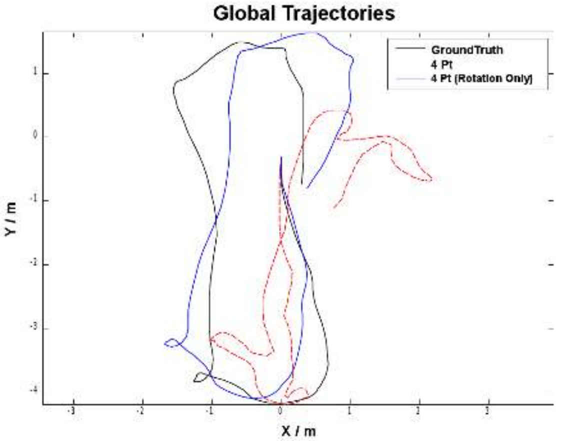

Fig. 11. Global trajectories from the 4-point algorithm (red dotted graph) and groundtruth (black graph) in the top view. The blue graph is the global trajectory computed with rotation values from the 4-point algorithm and remaining values from groundtruth.

be eliminated. In our implementation, the correct solution is the one from the remaining 2 solutions which gives the smallest difference in R when compared with the IMU readings.

Figure 10 shows plots of the relative rotation and translation values between consecutive keyframes (blue graphs) overlaid with the Vicon groundtruth (black graphs). For better comparison, the translation values from the 4-point algorithm and the groundtruth are normalized to unit length. Similar to the 5-point algorithm, the yaw measurements is very accurate with a high α value. The most interesting observation is that the 4-point algorithm failed to detect changes for roll, pitch and z directions. The failure of the 4-point algorithm to detect changes in the roll, pitch and z directions is probably because the relative changes in these directions are significantly smaller than the remaining directions.

Figure 11 shows the global trajectories from the 4-point algorithm (red dotted graph) and the Vicon groundtruth (black graph). Similar to the 5-point algorithm, the pair-wise transformations from the 4-point algorithm are concatenated to get the global trajectory. We scaled the translation vectors t with the groundtruth scale since we are only able to recover the relative scale from the 4-point algorithm. We observed that the global trajectories from the 4-point algorithm deviates significantly from the groundtruth. This deviation is mainly due to the erroneous translation values. The blue graph is the global trajectory with the rotation values from the 4-point algorithm and remaining values from the groundtruth. The similarity between the two trajectories shows that the yaw estimates from the 4-point algorithm are accurate.

C. Pose Estimation with ARToolKitPlus

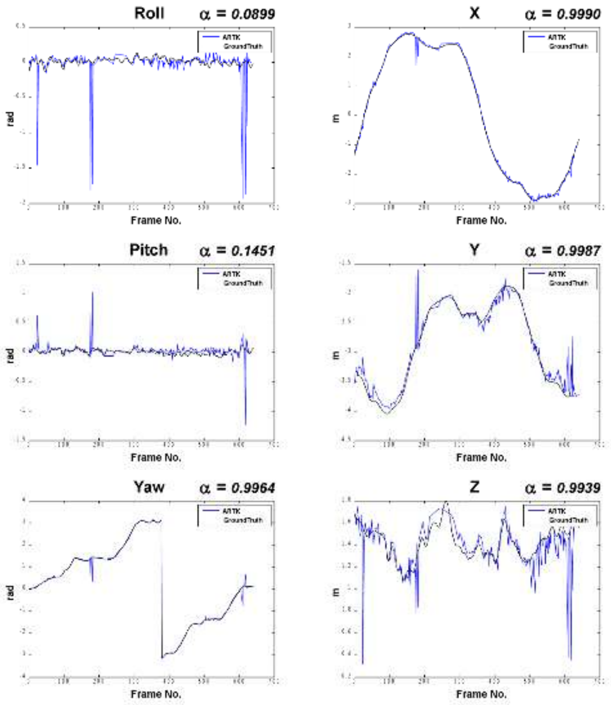

Fig. 12. Comparison of ARToolKitPlus measurements to ground truth. The plots show x, y, z, roll, pitch, yaw values for the 1LoopDown dataset. The translation values and yaw measurements are very precise with α values close to 1.

The final example that we show in this paper is the pose estimation results from the ARToolKitPlus software [14] as compared to the Vicon groundtruth. A group of 44 ARToolKitPlus markers was placed on the ground at known poses with respect to the reference frame of the Vicon system. This would allow us to obtain the pose of the MAV with respect to the

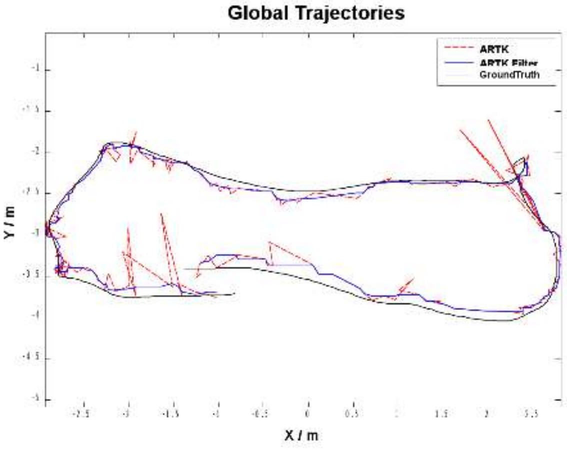

Fig. 13. Comparison of ARToolKitPlus pose estimates to ground truth (top view). The black graph is the groundtruth. A smoother trajectory after median filtering is shown by the blue graph.

reference frame of the Vicon system and direct comparison with the pose estimated from the Vicon system would be possible. Unlike the two previous examples which extracted keyframes, in this example we processed every single frame from the 1LoopDown dataset.

Figure 12 shows the comparison of the absolute rotation and translation values from ARToolKitPlus with the Vicon groundtruth (black graphs). It is clear from these plots and α values that the translation and yaw measurements from ARToolKitPlus (blue graphs) are very precise with the exception of occasional glitches. Roll and pitch measurements are significantly less accurate. This is probably due to the small changes which are harder to measure. Figure 13 shows the computed trajectory from the ARToolKitPlus software (red dotted graph) overlaid with the groundtruth from the Vicon system (black graph) in top view. We observed that the occasional glitches in the ARToolKitPlus pose estimate caused "jumps" to the trajectory. Nevertheless, the problem of occasional glitches in the ARToolKitPlus pose estimate can be easily alleviated by smoothing the estimates with a median filter (in this example, size=5). The blue graph in Figure 13 shows the estimated trajectory after filtering. The filtered trajectory is obviously smoother and closer to the groundtruth.

VI. CONCLUSIONS

In this paper, we have pointed out the need for a new benchmarking toolset for evaluating pose estimation algorithms on MAVs. We have created synchronized datasets from a forward looking camera, a downward looking camera and IMU on a quadrotor platform, and groundtruth from the Vicon system. We have also showed examples of using these datasets for benchmarking some existing visual pose estimation algorithms. Our datasets are made available for public access with the hope that they could be useful for future researchers working on pose estimation algorithms on MAVs.

ACKNOWLEDGMENTS

This work is part of the sFly project, funded by the European Community's Seventh Framework Programme (FP7/2007-2013) under grant agreement #231855. It is also partially supported by the Swiss National Science Foundation (SNF) under grant number #200021-125017. The authors would like to thank Professor D'Andrea Raffaello and Sergei Lupashin from the Institute of Dynamic Systems and Control at ETH Zürich for providing the Vicon system and giving assistance with the Vicon data collection.

REFERENCES

[1] Andrea Bonarini, Wolfram Burgard, Giulio Fontana, Matteo Matteucci, Domenico Giorgio Sorrenti and Juan Domingo Tardos, "RAWSEEDS: Robotics Advancement through Web-publishing of Sensorial and Elaborated Extensive Data Sets", *in proceedings of IROS'06 Workshop on Benchmarks in Robotics Research*, 2006.

[2] Cyrill Stachniss, Udo Frese and Giorgio Grisetti, "OpenSLAM.org", http://openslam.org/.

[3] Andrew Howard and Nicholas Roy, "The Robotics Data Set Repository (Radish)", http://radish.sourceforge.net/, 2003.

[4] Willow Garage, "ROS - Robotics Open Source", http://www.ros.org.

[5] Hugh Durrant-Whyte and Tim Bailey, "Simultaneous Localization and Mapping: Part I", *in IEEE Robotics and Automation Magazine*, June 2006.

[6] Hugh Durrant-Whyte and Tim Bailey, " Simultaneous Localization and Mapping: Part II", *in IEEE Robotics and Automation Magazine*, June 2006.

[7] Thrun, S. and Burgard, W. and Fox, D., "Probabilistic Robotics", *MIT Press*, 2005.

[8] Paul Newman and Kin Ho, "SLAM-Loop Closing with Visually Salient Features", *in Proceedings of the IEEE International Conference on Robotics and Automation (ICRA)*, 18-22 April 2005.

[9] Andrew J. Davison, Ian Reid, Nicholas Molton and Olivier Stasse, "MonoSLAM: Real-Time Single Camera SLAM"', *in IEEE Transactions on Pattern Analysis and Machine Intelligence (PAMI)*, 2007.

[10] Agrawal, M., and Konolige K., "FrameSLAM: From Bundle Adjustment to Real-Time Visual Mapping", *in IEEE Transactions on Robotics*, October 2008

[11] Bouguet, J., "Camera calibration toolbox for Matlab", 2006. http://www.vision.caltech.edu/bouguetj/calib_doc/htmls/parameters.html

[12] Scaramuzza, D., Martinelli, A. and Siegwart, R., "A Toolbox for Easy Calibrating Omnidirectional Cameras", *in Proceedings to IEEE International Conference on Intelligent Robots and Systems (IROS)*, October 7-15, 2006.

[13] Scaramuzza, D., Martinelli, A. and Siegwart, R., "A Flexible Technique for Accurate Omnidirectional Camera Calibration and Structure from Motion", *in Proceedings of IEEE International Conference of Vision Systems (ICVS)*, New York, January 5-7, 2006.

[14] Wagner Daniel, Schmalstieg Dieter, "ARToolKitPlus for Pose Tracking on Mobile Devices", *Proceedings of 12th Computer Vision Winter Workshop*, February 2007.

[15] D. Nister, "An efficient solution to the five-point relative pose problem", *in Proceedings IEEE Computer Society Conference on Computer Vision and Pattern Recognition (CVPR 2003)*, Volume 2, pages. 195-202, 2003.

[16] Fischler, Martin A. and Bolles, Robert C.,"Random sample consensus: a paradigm for model fitting with applications to image analysis and automated cartography", *in Readings in computer vision: issues, problems, principles, and paradigms*, 1987, pp. 726–740.

[17] David G. Lowe, "Distinctive image features from scale-invariant keypoints", *in International Journal of Computer Vision*, 2004, pp. 91-110.

[18] Yi Ma, Stefano Soatto, Jana Kosecka, and Shankar S. Sastry, "An invitation to 3-D vision: From images to geometrical approaches", *Springer-Verlag*, November 2003.

[19] Hartley, R. I. and Zisserman, A., "Multiple View Geometry in Computer Vision", Second Edition, *Cambridge University Press*, 2004.